Paper # 38PAH-0033 **Topic: Soot Formation** SAND2018-3006C

Western States Section of the Combustion Institute - Spring 2018 Meeting
Hosted by Oregon State University
March 25-27, 2018.

LES Soot-Radiation Predictions of Buoyant Fire Plumes

Heeseok Koo[1*] *John C. Hewson*[1] *Robert C. Knaus*[2]

[1]*Fire Science and Technology, Sandia National Laboratories, PO Box 5800, MS 1135, Albuquerque, NM 87185-1135, USA* [†]

[2]*Compuational Thermodynamics and Fluid Mechanics, Sandia National Laboratories, PO Box 5800, MS 0828, Albuquerque, NM 87185-0828, USA*

This study addresses predicting the internal thermochemical state in buoyant fire plumes using large-eddy simulations (LES) with a tabular flamelet library for the underlying flame chemistry. Buoyant fire plumes are characterized by moderate turbulent mixing, soot growth and oxidation and radiation transport. Soot moments, mixture fraction and enthalpy evolve in the LES with soot source terms given by the non-adiabatic flamelet library. Participating media radiation transport is predicted using the discrete ordinates method with source terms also from the flamelet library, and the LES subgrid-scale modeling is based on a one-equation kinetic-energy sub-filter model. This library is generated with flamelet states that include unsteady heat loss through extinction nominally representing radiative quenching. We describe the performance of this model both in the context of a laminar coflow configuration where extensive measurements are available and in buoyant turbulent fire plumes where measurements are more global.

1 Introduction

Soot is known to evolve slowly relative to most of the main combustion chemistry [1] so that quasi-steady assumptions, as typical in flamelet modeling, for example, are not generally accurate for predicting soot volume fractions. However, those components of the soot source terms that depend on the main flame chemistry have been expressed using flamelet libraries with some success [2, 3]. This led to a series of two-equation soot models being developed on a semi-empirical basis [4, 5, 6], which were applied to both Reynolds-averaged Navier-Stokes (RANS) and LES [2, 3, 7, 8, 9, 10, 11].

Since soot evolution is sensitive to the temperature, the accurate prediction of the flame temperature is required. Typically, radiative heat losses are introduced as an additional parameter for the flamelet model when a sooting flame is modeled [8, 12]. With heat losses, solutions above the middle branch of the so-called S-curve can exist as quasi-steady state solutions, but these retain the characteristics of burning flames. In strongly radiating flames, heat losses may significantly weaken a flame so that soot oxidation is inhibited, leading to smoke emissions. In the present work, which focuses on strongly sooting and radiating flames, the heat loss is incorporated into

*Corresponding author: hkoo@sandia.gov

†Sandia National Laboratories is a multimission laboratory managed and operated by National Technology and Engineering Solutions of Sandia, LLC, a wholly owned subsidiary of Honeywell International, Inc., for the U.S. Department of Energy's National Nuclear Security Administration under contract DE-NA0003525.

an unsteady flamelet evolution that allows a flame state to be described below the S-curve middle branch and down to arbitrary temperatures suitable also for heat transfer to cool surfaces, for example. Within the RANS or LES simulation, an enthalpy transport equation that accounts for the radiative and wall heat losses is solved with the resulting enthalpy being one independent variable for the flamelet state.

In the present work, we couple the non-adiabatic flamelet with a discrete-ordinate based radiation model for an accurate description of an interaction between radiation and soot fields. The model is tested on a laminar jet and a buoyant-driven fire plume.

2 Soot-Radiation Modeling

Simulations of the flow field for both laminar and turbulent flows are conducted using Fuego, an unstructured low-Mach number turbulent combustion code that is a component of Sandia National Laboratories' SIERRA thermal-fluids code suite [13]. Within Fuego several RANS and LES turbulent models are available as are combustion models based on both flamelet concepts and the eddy-dissipation concept. For the present study, we will employ either a laminar flow assumption or use the k-SGS model for LES [14, 15] while the main flame chemistry (hydrocarbon fuel oxidation to final products except soot) is modeled using the flamelet concept coupled with evolved variables that represent soot. For the sake of brevity, the basic filtered Navier-Stokes equations are not presented here. For the same reason, filtering notation is omitted in many equations in the following sections. In addition to the soot evolution described in the next subsection, equations for the Favre-filtered mixture fraction, $\tilde{Z}$, and enthalpy, $\tilde{H}$, evolve with the Navier-Stokes equations under the selected filtering process.

We note that we do not solve a progress variable in the sense that describes the overall chemical-energy release as is done in some approaches to flamelet modeling for high dissipation-rate flames subject to local extinction [16, 17]. For the present low dissipation-rate scenarios, the radiative heat loss drives the change in the flame state and the enthalpy is the more appropriate progress variable for the main flame chemistry. This is discussed further in the sections that present simulation results. The soot evolution described below does follow the same general approach as progress-variable approaches [8, 12] with source terms derived from the non-adiabatic flamelet library as described throughout the paper.

The enthalpy equation has a source term associated with radiative heat transfer and the source term is computed using another component of the SIERRA thermal-fluids code suite known as Syrinx [13]. Syrinx solves the radiative transfer equation in the grey-gas limit with angular discretization using the discrete ordinates model; here, at least 72 directions are solved to determine radiative fluxes.

$$\frac{\partial \rho H}{\partial t} + \nabla \cdot (\rho \mathbf{u} H) = \nabla \cdot (\rho D \nabla H) - (4a\sigma T^4 - aG) \tag{1}$$

The last two terms are associated with the emission and absorption of radiant flux, respectively. σ is the Stefan Boltzmann constant, and a is the absorption coefficient, which depends on species composition and amount of the soot. G is the spherically integrated flux of all participating ordinates $G = \int I(s) d\Omega$, where $I(s)$ is the radiation intensity along the direction s. The Boltzmann

radiative transport equation is solved to determine the intensity along each direction s

$$s \cdot \nabla I(s) + aI(s) = e \tag{2}$$

where s is in the unit vector length and e is the radiative emission. a and e are separated into the gas-phase and soot contributions such that $a = a_{gas} + a_{soot}$ and $e = e_{gas} + e_{soot}$. a_{gas} is computed using curve fits to the results of RADCAL for the gas-phase species CO, CO_2, H_2O and CH_4 [18, 19]. Soot absorption is modeled as follow [20].

$$a_{soot} = (-375000 + 1735T)\rho M/\rho_{SOOT} \tag{3}$$

As will be further discussed in Sec. 2.1, ρM is the soot mass concentration and ρ_{SOOT} is the density of the soot particle. Radiative emission terms are $e_{gas} = a_{gas}\sigma T^4/\pi$ and $e_{soot} = a_{soot}\sigma T^4/\pi$. These absorption coefficients and radiative emission terms terms are precomputed using the non-adiabatic flamelet library. Soot contributions are stored per soot mass concentration.

For heavily sooting fires the fraction of the mixture fraction that becomes associated with the soot is significant, and in the current work the mixture fraction is to be associated with the gas phase. In this case, a source term is required for the mixture fraction phase which is the *opposite* of the soot mass density source term given in the next section, or the right hand side of Eq. 5 sans the viscous term. We currently assume that the interconversion between mixture fraction and soot does not alter the enthalpy content.

In addition to the source terms indicated above and described below, the non-adiabatic flamelet library provides the density, temperature, specific heat and viscosity as a function of the input variables. The full vector of input variables employed is described in detail in Sec. 2.2

2.1 Soot evolution equations

For the present demonstration we use a two-equation soot model, transporting both the number density (ρN) of soot and the mass concentration (ρM), to describe the development of soot.

$$\frac{\partial \rho N}{\partial t} + \nabla \cdot (\rho \mathbf{u} N) = \nabla \cdot \left(\frac{\mu}{\mathrm{Sc_{soot}}} \nabla N \right) + (\mathrm{Nucl.}) - (\mathrm{Coag.}) \tag{4}$$

$$\frac{\partial \rho M}{\partial t} + \nabla \cdot (\rho \mathbf{u} M) = \nabla \cdot \left(\frac{\mu}{\mathrm{Sc_{soot}}} \nabla M \right) + W_p(\mathrm{Nucl.}) + [(\mathrm{Surf.}) - (\mathrm{Oxid.})]\, A \tag{5}$$

To use the established universal transport equation solver in Fuego, we define N and M so that density weighted parameters are the soot number density and mass concentration. That is, M is the soot mass fraction and N is the soot number per mass mixture (carried in kmol/kg unit for numerical accuracy). The soot Schmidt number $\mathrm{Sc_{soot}}$ is set to be large enough that soot fields are non-dissipative in laminar flow; this is not true in turbulent flows where the standard turbulent Schmidt number is employed, $\mathrm{Sc_t} = 0.9$.

The source terms refer to the nucleation, coagulation, surface growth, and oxidation processes and are modeled according to the parameters given by [3, 6, 21]. The oxidation terms include both

oxygen and OH contributions. $W_p = 144$ kg/kmol in Eq. 5 is the molecular weight of a soot nucleate.

$$(\text{Nucl.}) = 54 N_A \frac{X_{C_2H_2} P}{R_0 T} e^{-21100/T} \tag{6}$$

$$(\text{Coag.}) = \left(\frac{24 R_0 T}{\rho_{SOOT} N_A} \right)^{1/2} d_p^{1/2} (\rho N)^2 \tag{7}$$

$$(\text{Surf.}) = 11700 \left(\frac{X_{C_2H_4} P}{R_0 T} \right) e^{-12000/T} \tag{8}$$

$$(\text{Oxid.}) = 500 \frac{X_{O_2} P}{R_0 T} T^{1/2} e^{-20000/T} + 4.2325 \frac{X_{OH} P}{R_0 T} T^{1/2} \tag{9}$$

N_A is the Avogadro's number, R_0 is the universal gas constant, soot density $\rho_{SOOT} = 1800$ kg/m^3, and X is the mole fraction. Using a spherical particle assumption, the averaged particle diameter d_p is

$$d_p = \left(\frac{6M}{\pi N \rho_{SOOT}} \right)^{1/3} \tag{10}$$

and the total surface area A is

$$A = \rho N \pi d_p^2 \tag{11}$$

The soot equations evolve with the source terms, absent the dependence on N and M, tabulated through the non-adiabatic flamelet library described below.

2.2 Flamelet library structure

In the flamelet model approach, required variables such as temperature, density, and source terms for radiation and soot are obtained using a mapping between the slowly evolving variables that are evolved with the fluid flow and the fast-evolving variables that are precomputed using the approach given in the next section. For a laminar flamelet with strong radiative losses, the slowly evolving variables are the filtered mixture fraction and enthalpy, $\tilde{Z}$ and $\tilde{H}$. In addition, the library variables depend on the local mixing rate; the scalar dissipation rate, $\tilde{\chi}$, the rate of molecular dissipation of the mixture fraction, provides this mixing rate.

Finally, for turbulent flows where the mixture fraction is not well resolved, the mixture fraction variance, $\widetilde{Z''^2}$, is an input to the library. A presumed probability density function (PDF) approach using either a clipped-Gaussian-PDF or beta-PDF is used, and all output variables are convolved over the given PDF, which is a function of $\tilde{Z}$ and $\widetilde{Z''^2}$. This integration accounts for the so-called turbulence-chemistry interaction and turbulence-radiation interaction under the assumption that the chemical sources and radiative sources are strongly correlated with the mixture fraction. However, because we use values for N and M from the evolution equations in the soot source terms, the interactions in the fluctuations of N and M with the fluctuations in the reaction rate coefficients are ignored.

Nominally, the enthalpy and scalar dissipation rate are also subject to convolution over a PDF in those directions, but the assumption is made that a delta function PDF can be employed and that the conditional dependence on the mixture fraction is exactly that given by the flamelet equations.

For the enthalpy, this can be justified by the more rapid variation of most terms in the mixture fraction direction and the initial correlation of the enthalpy with the mixture fraction. For the scalar dissipation rate the justification is different: far from extinction the dependence on the dissipation rate is not large and the variation of the dissipation rate in time is fast relative to the rate of the flamelet response to that variation so a quasi-steady structure is assumed with dissipation rate fluctuations about $\tilde{\chi}$.

We note that the library is constructed using an enthalpy deficit, γ, defined as the difference between the enthalpy and the adiabatic enthalpy, $H_{ad}(Z)$; the latter is initially linear in Z in the unity Lewis number approximation

$$H_{ad} = H(0) + [H(1) - H(0)]\, Z \qquad \text{and} \qquad \widetilde{H_{ad}} = H(0) + [H(1) - H(0)]\, \tilde{Z} \tag{12}$$

so that

$$\gamma = H - H_{ad} \qquad \text{and} \qquad \tilde{\gamma} = \tilde{H} - \widetilde{H_{ad}} \tag{13}$$

where H and $\tilde{H}$ are the variables evolved by the laminar flow/flamelet equations and the turbulent filtered conservation equations, respectively, and γ and $\tilde{\gamma}$ are the laminar and turbulent flamelet library dependent variables. While the adiabatic enthalpy represents simple mixing between the fuel and oxidizer enthalpy states, it can differ slightly from the mixture fraction because we include a mixture fraction source term associated with the soot mass and neglect this contribution to the enthalpy.

2.3 Non-adiabatic flamelet generation

The generic flamelet equation for scalar ϕ with source term $\dot{\omega}$ is written

$$\frac{\partial \phi}{\partial t} + \frac{\chi}{2}\frac{\partial^2 \phi}{\partial Z} = \dot{\omega}. \tag{14}$$

Of interest here is the treatment of the non-adiabatic contribution to the energy equation. As noted in the Introduction, for flame states above the S-curve middle branch, it is possible to generate a steady-state flamelet with heat losses, and this approach has been employed before [8, 12]. However, in fires, radiative heat losses can lead to lower temperatures and interactions with cold surfaces can lead to local temperatures very near ambient.

While the temperature equation is actually the equation solved for the energy in the flamelet, it is easier to express the nonadiabatic evolution using the enthalpy which is the variable transported by Fuego. The flamelet enthalpy equation is written

$$\frac{\partial H}{\partial t} + \frac{\chi}{2}\frac{\partial^2 H}{\partial Z} = h(\chi, T_{max})\,[T(H, Z) - T_\infty] \tag{15}$$

where T_∞ is the temperature of the surroundings, and the right-hand side source term is expressed as a heat loss using a heat transfer coefficient, $h(\chi, T_{max} - T_\infty)$. Here the heat loss is linear in the temperature, though it could also be expressed using the fourth power of the temperature to mimic radiant heat losses. For reasons detailed below, we recommend using a linear dependence on temperature if the objective is to generate flamelets cooled to near ambient temperatures.

Before detailing the heat-loss source terms, we note some characteristics of Eq. 15. First, it is desirable to have lower temperatures associated with reduced enthalpy. This is true only when the chemical mixing of reactants occurs slower than the heat losses. While the flame is burning (above the S-curve middle branch) the enthalpy of reactant mixing is converted to sensible enthalpy that is subject to cooling, but once the flame is cooled to temperatures below the S-curve middle branch mixing of reactants tends to increase the stoichiometric enthalpy. For the enthalpy to continue to be reduced ($\partial H/\partial t < 0$) it is necessary that the heat loss term be larger in magnitude than the enthalpy dissipation term, $(\chi/2)\,(\partial^2 H/\partial Z)$. This leads to two considerations:

- It is necessary to have a larger heat loss when χ is larger in order to overcome the increased magnitude of the dissipation term. This leads us to scale the heat loss coefficient by χ.
- It is desirable that the heat loss term not be appreciably slower for low temperatures to avoid reactant mixing leading to increases in stoichiometric enthalpy. This has led us to adopt the linear temperature dependence appearing in the right-hand side of Eq. 15, and also to scale the heat loss by $(T_{max} - T_\infty)^{-1}$.

The final expression for the heat transfer coefficient is

$$h(\chi, T_{max}) = h_0 \chi \,(T_{max} - T_\infty)^{-1} \tag{16}$$

where h_0 is a sufficiently large value to overcome the chemical heat release (proportional to χ in non-premixed combustion). It is certainly possible to consider other combinations, including a T^4 dependence, but the authors have found that this expression has nice properties.

2.4 Flamelet library construction

A flamelet library is generated using a modified version of the FlameMaster code [22] using a two-stage generation process. The first stage consists of generating a set of steady-state flamelet solutions (with $Z \in [0, 1]$) over the range of boundary compositions, pressure and enthalpy that are relevant and for the range of dissipation rates that are relevant. In the present case, the former boundary conditions are air and ethene at ambient pressures and boundary temperatures, but multiple mixture fractions and enthalpy ranges can be specified. The dissipation rates extend from near extinction to low values below which there is little change in properties; $\chi = 0.01$ s^{-1} is typical. It is effective to allow χ to vary geometrically.

The second stage consists of a transient flame evolution from the full set of steady-state solutions under strong heat loss conditions described above. The flamelet state is solved at the initial steady-state condition and periodically during this transient evolution. For the current case, a state is saved each time the stoichiometric enthalpy is reduced by approximately 2.5e4 kJ/kg until the flame reaches the surrounding temperature.

The two-stage process is demonstratedin Fig. 1. The upper curve represents the locus of steady-state solutions as a function of χ along the upper S-curve branch. From every steady-state solution, transient evolution leads to a sequence of flamelets at lower maximum flame temperatures until a temperature around $T_\infty + 5$ K. In this manner the heat-loss term described in the previous subsection

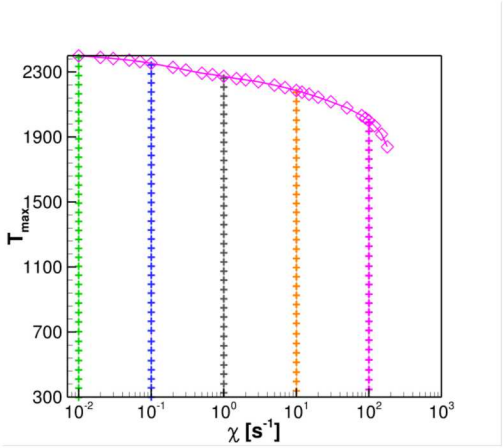

Figure 1: The maximum flame temperatures associated with various individual flamelet files that contribute to the flamelet library are shown. The top curve shows states associated with steady-state flamelets and vertical trajectories show unsteady flamelet evolution. Only a subset of states are shown: there are six logarithmically spaced states per decade of χ and a state roughly every 2.5e4 kJ/kg for the stoichiometric point (≈25 K change in T_{max}).

allows the generation of a library that covers the full range from the upper branch to near the lower frozen-mixing branch. Note, however, that this lowest temperature solution is not pure mixing because that would have fuel and oxidizer giving an enthalpy equal to the adiabatic flame. This lowest temperature state is rapidly cooled products with modest reactant mixing. Example enthalpy and temperature profiles that result from one single initial χ value are given in Fig. 2.

Observing the process also provides some insight into the evolution of rapidly cooled flames. In Fig. 3 the stoichiometric enthalpy and maximum flame temperature are plotted as a function of normalized time (using the stoichiometric χ) during the cooling process. It is seen that the selected heat transfer form yields enthalpy trajectories that are similar, but the temperature trajectories differ due to the nature of the S-curve. The change in slope for the temperature trajectories is associated with crossing below the S-curve middle branch whence chemical heat release becomes negligible. Flames at lower χ are initially hotter as expected, but this continues, and they are consistently hotter for a fixed H_{st}; this last behavior is associated with less reactant leakage for smaller χ.

2.5 Tabulation

As discussed above, in the the non-adiabatic flamelet library, thermochemical variables, soot sources and radiation source terms are obtained as a function of $\tilde{Z}$, $\widetilde{Z''^2}$, $\tilde{\chi}$, and $\tilde{\gamma}$. Since soot sources and radiation parameters are a complex function of temperature and species composition (Eqs. 3-5), pre-computing and storing a lookup table saves computational cost. In LES, the mixture fraction variance which represents the subfilter distribution and the scalar dissipation is related to the mixing efficiency, which are approximated as

$$\overline{\rho}\widetilde{Z''^2} = C_V \overline{\rho}\Delta^2 \frac{\partial Z}{\partial x_i}\frac{\partial Z}{\partial x_i} \tag{17}$$

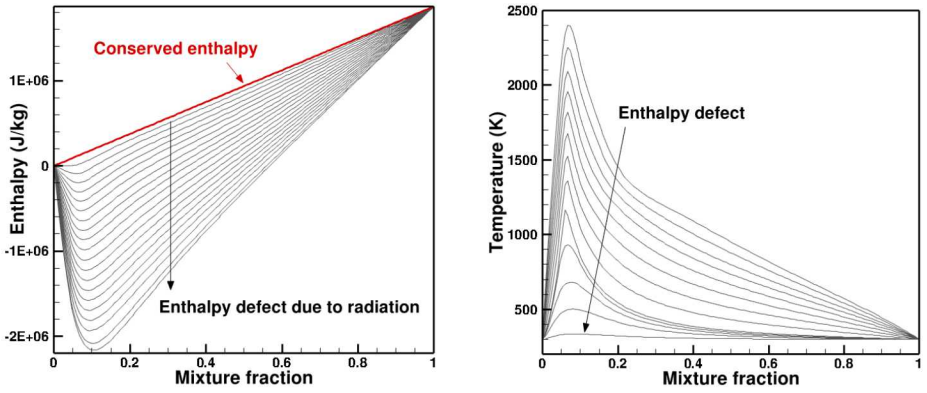

Figure 2: Enthalpy and temperature profiles for a sequence of unsteady flamelet calculations starting with an adiabatic state and cooling to near ambient temperatures, at $\chi = 0.01$. Only a subset of states are shown.

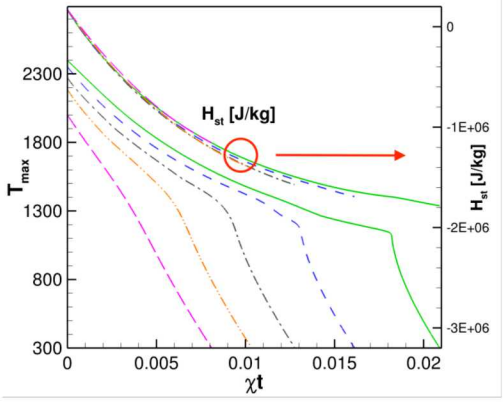

Figure 3: The stoichiometric enthalpy and maximum flame temperature are plotted as a function of normalized time (using the stoichiometric χ) during the cooling process. From left to right, curves correspond to $\chi = 100$, 10, 1, 0.1, 0.01 s^{-1}.

$$\tilde{\chi} = 2(D + D_t)\frac{\partial Z}{\partial x_i}\frac{\partial Z}{\partial x_i} \tag{18}$$

for which a dynamic procedure is involved to calculate the model coefficient C_V in the simulations [23, 24].

To optimize the access speed and the structure of the library, the dependent variables are converted largely to a structured form. The scalar dissipation is stored using its stoichiometric value, and $\tilde{\chi}$ is converted to the stoichiometric value using a theoretical profile, $\chi = \chi_{|Z=0.5}\exp\left(-2\left[\mathrm{erfc}^{-1}(2\mathrm{Z})\right]^2\right)$. This removes interpolation errors associated with an additional interpolation in scalar dissipation dimension while tabulating the flamelets. The mixture fraction variance is non-dimensionalized by the maximum possible variance at the given mixture fraction $Z(1-Z)$ with logarithmically spaced values to provide better resolution at small variances typical of LES.

The library is generated over a broad range of the dependent variable space, but particularly in the scalar-dissipation coordinate it is possible to exceed the values for which the the independent variables were evaluated. In the case of extrapolation, the value at the end of the table in the given direction is copied to further values in the extrapolation direction.

As an example of the resulting library, Fig. 4 shows temperature contours over a range of mixture fraction and dissipation rates. The various planes are various magnitudes of the enthalpy loss, expressed in terms of the stoichiometric values γ_{st} or equivalently the H_{st}. The range of γ_{st} is from adiabatic to fully cooled ($T \approx T_\infty$). This library corresponds to $\widetilde{Z''^2} = 0$ or a laminar case. In general another library dimension exists over which $\widetilde{Z''^2}$ varies, but this is not shown for simplicity.

For this library in Fig. 4 the dependent variable evaluation for values of χ beyond the limits of the initial library is also shown; this corresponds to the extrapolation described in the previous paragraph. For extrapolation at small values of χ that occur frequently in fire calculations, there is negligible evident consequence associated with the extrapolation. For large values of χ that exceed the critical extinction condition (not generally seen in fires), the prediction is poor since these might nominally show a transition to extinguished temperatures. When χ is expected to exceed the critical extinction value, the previously described approaches using a flamelet progress variable would generally be preferable.

3 Evaluation on a Laminar Flame

The model was evaluated on an ethylene laminar coflow, sooting jet following an experimental design using the Santorro burner [25] with measurements available in Ref. [26]; the present case is referred to as C2H4-40. The diameter of the laminar jet is 11mm, and the bulk velocity is 3.98 cm/s assuming a jet exit temperature of 300 K for the given mass flow rate. The coflowing air velocity is higher at 8.9 cm/s. A fully developed laminar velocity profile is assumed at the jet exit while a constant velocity profile is provided for the coflow, which is supported by a flow-straightening structure installed in the coflow section of the experiment [25]. The inlet temperature is fixed at 300K for both streams. While follow-up experiments reported a higher temperature at the jet exit due to heating from the flame [26], the effect is ignored in the simulation. To use our radiation solver, a three-dimensional domain was used despite the axisymmetric nature of the

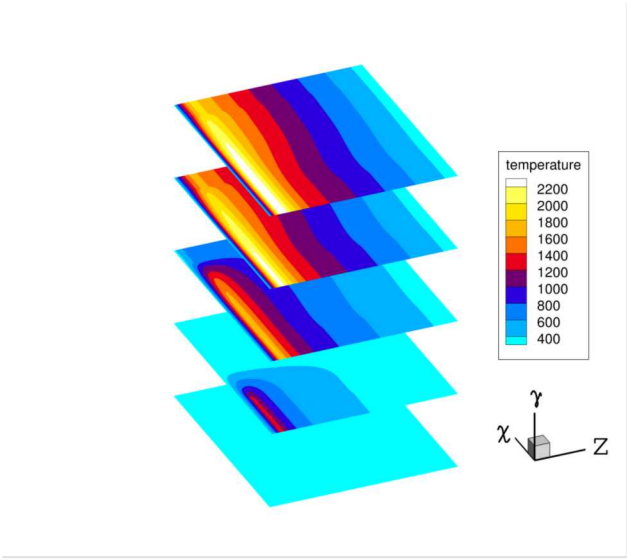

Figure 4: Surfaces associated with a laminar ($\widetilde{Z''^2} = 0$) flamelet library are evaluated from a flamelet library for C_2H_4. In the χ direction, the evaluation extends beyond the input range of values as discussed in the text.

flame. A total of 200,000 mesh points are used, but considering 10 cells were used to discretize in azimuthal directions, the grid is equivalent to a 20,000 2-D mesh. A 3-D flamelet library, leaving out $\widetilde{Z''^2} = 0$, is used in the laminar flame simulation.

Predicted contours of temperature, soot volume fraction, mixture fraction, and enthalpy deficit are presented in Fig. 5. The magnitude of the effect of radiation on the enthalpy deficit is clearly seen as the flow moves downstream and the temperature decreases. Radial profiles of velocity, temperature, and soot mass fraction at selected downstream locations are compared to the experiment data at Fig. 6. While the velocity and temperature profile match the experiment relatively well, soot growth is initiated earlier, and soot is not fully oxidized given the current mechanism. Figure 7 shows that as much as 13% of the fuel was converted to soot, resulting in 8.34ppm as the maximum soot volume fraction observed in the simulation.

While the oxidation model needs further investigation, the maximum soot volume fraction is in reasonable agreement with the experiment, which lets us move to a buoyant turbulent flame.

4 Sooting Fire Plume

Using the model evaluated on the laminar case, a sooting turbulent fire plume was simulated where ethylene is the fuel. Similar flames have been measured at Sandia National Laboratories in the FLAME facility, an indoor controlled test facility for meter scale fires [27] (Fig. 8). Flow conditions follow other FLAME facility measurements [28, 29]. A simplified cylindrical computational domain was used with fuel and air coflow velocities given as 0.097 and 0.14m/s. Three mesh resolutions were used where the smallest mesh size is approximately 1cm, 2cm, or 4cm; the mesh is gradually coarsened away from the plume. Results from the most refined mesh (smallest size of 1cm; total mesh elements of 7 million) are presented here.

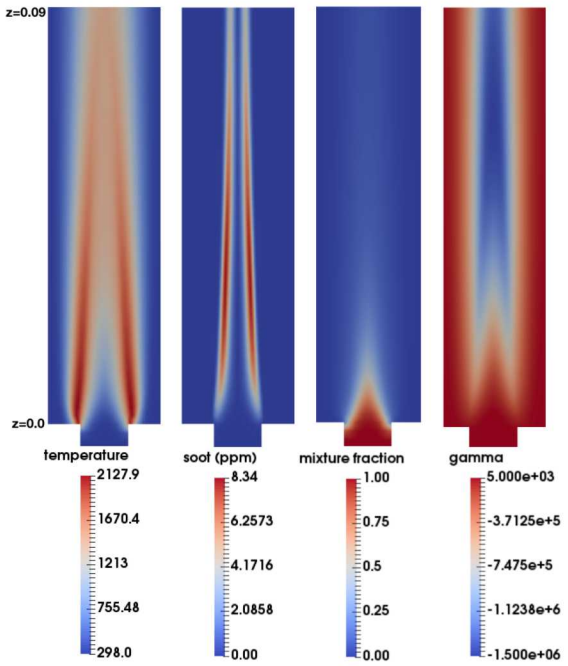

Figure 5: Overall flowfield for the coflowing laminar jet simulation.

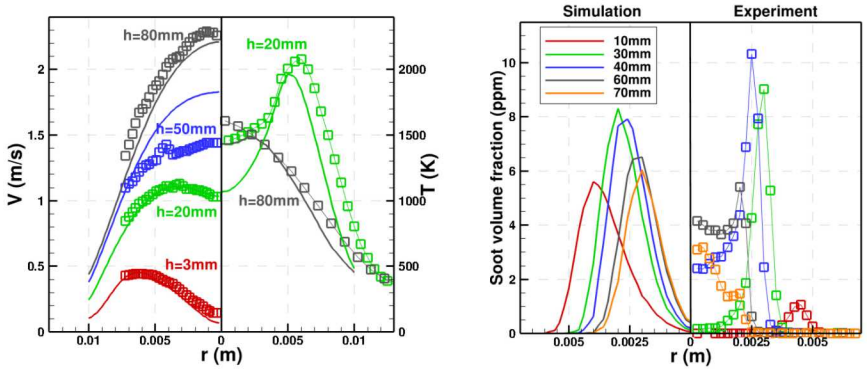

Figure 6: Velocity, temperature, and soot volume fraction radial profiles in the laminar jet (lines) compared to the experiment (boxes)

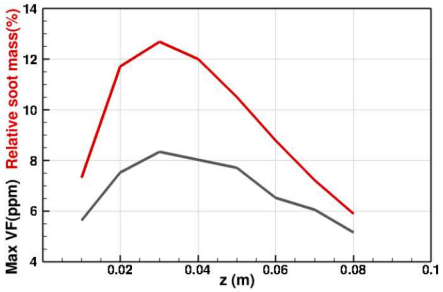

Figure 7: Relative soot mass compared to the fuel mass (red), and maximum of soot volume fraction (black) at different heights

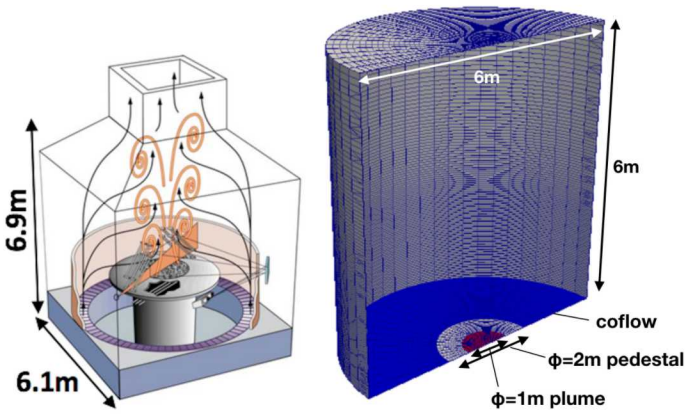

Figure 8: FLAME facility and the computational domain

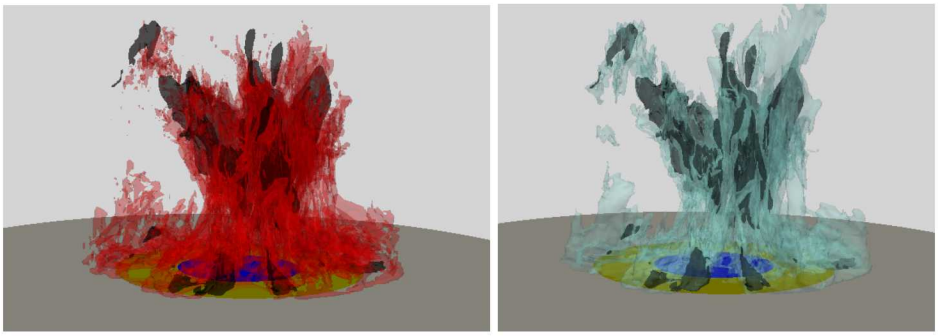

Figure 9: Instantaneous isocontours of soot at 10ppm (black), temperature at 1400K (red), mixture fraction at stoichiometric (light blue).

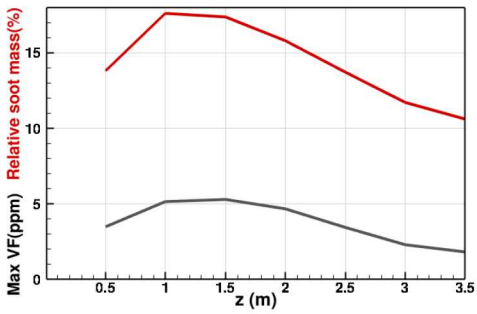

Figure 10: Relative soot mass compared to the fuel (red), and maximum of averaged soot volume fraction (black) at different heights.

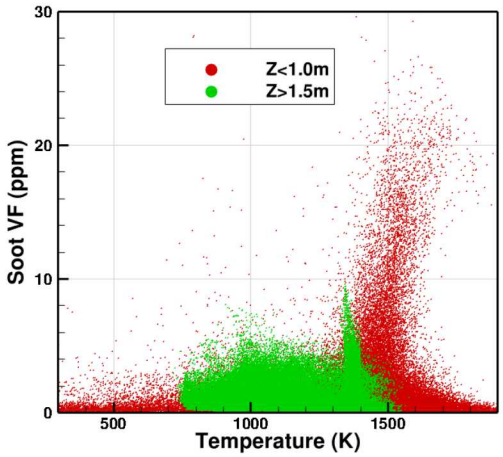

Figure 11: Instantaneous scatter plot of soot versus temperature. Red dots indicate upstream while green dataset is from downstream.

Figure 9 shows instantaneous isocontours of mixture fraction, temperature and soot volume fraction. The soot field is highly intermittant in the plume. While the averaged field is not fully converged yet, some initial statistics are reported. The amount of soot relative to the fuel is higher than the laminar case in the previous section, and now peaks at close to 18% (Fig. 10). To demonstrate the role of the flamelet library in the evolution of the soot and enthalpy states Fig. 11 shows a scatter plot of the soot and temperature conditionally sampled for mixture fraction values between 0.03 and 0.1 and from different regions, below 1m and above 1.5m. When soot is increasing low in the flame, the soot volume fraction is positively correlated with temperature since higher temperatures promote soot growth. Meanwhile, as the green points indicate, when soot levels are decreasing higher in the flame, the soot volume fraction is somewhat negatively correlated with temperature due to enhanced oxidation at higher temperatures.

5 Conclusion

We describe an unsteady flamelet approach to developing a non-adiabatic flamelet library. The transient approach allows the flame temperatures to range from adiabatic to the temperatures of the surroundings, allowing treatment of both radiation heat transfer and wall heat transfer. Source terms for a two-equation soot model are implemented in the context of this non-adiabatic flamelet library. The formulation is evaluated using a laminar ethene flame, with subsequent predictions of a sooting turbulent fire plume underway. For the laminar ethene flame, the model predicts the maximum soot volume fraction with reasonable accuracy, but oxidation is underpredicted. Preliminary results of a sooting pool fire simulation are also introduced.

References

[1] J. H. Kent and D. Honnery. *Combustion Science and Technology*, 54 (1987) 383–398.

[2] J. J. Young and J. B. Moss. *Combustion Science and Technology*, 105 (1995) 33–53.

[3] S. J. Brookes and J. B. Moss. *Combustion and Flame*, 116 (1999) 486–503.

[4] K. M. Leung, R. P. Lindstedt, and W. Jones. *Combustion and Flame*, 87 (1991) 289–305.

[5] P. R. Lindstedt. Simplified soot nucleation and surface growth for nonpremixed flames. In H. Bockhorn, editor, *Soot Formation in Combustion*, Vol. 59 of *Chemical Physics*, pages 417–439. Springer- Verlag, 1994.

[6] I. Aksit and J. Moss. *Combustion and Flame*, 145 (2006) 231–244.

[7] H. Pitsch, E. Riesmeier, and N. Peters. *Combustion Science and Technology*, 158 (2000) 389–406.

[8] M. E. Mueller and H. Pitsch. *Physics of Fluids*, 25 (2013) 110812.

[9] Y. Xuan and G. Blanquart. *Proceedings of the Combustion Institute*, 35 (2015) 1911–1919.

[10] H. Koo, M. Hassanaly, V. Raman, M. E. Mueller, and K. P. Geigle. *Journal of Engineering for Gas Turbines and Power*, 139 (2017) 031503.

[11] A. Chong, M. Hassanaly, H. Koo, V. Raman, K. P. Geigle, and M. E. Mueller. *Combustion and Flame*, (2018) Accepted.

[12] M. Ihme and H. Pitsch. *Physics of Fluids*, 20 (2008) 055110.

[13] Sandia National Laboratories. *SIERRA Low Mach Module: Fuego User Manual – Version 4.42, SAND2016-10164*, 2016.

[14] S. Menon and W. W. Kim. High reynolds number flow simulations using the localized dynamic subgrid-scale model. In *AIAA 34th Aerospace Sciences Meeting and Exhibit*, number AIAA1996-0425, 1996.

[15] X. Chai and K. Mahesh. *Journal of Fluid Mechanics*, 699 (2012) 385–413.

[16] C. D. Pierce and P. Moin. *Journal of Fluid Mechanics*, 504 (2004) 73–97.

[17] M. Ihme, C. Cha, and H. Pitsch. *Proceedings of the Combustion Institute*, 30 (2005) 793–800.

[18] W. L. Grosshandler. Radcal: A narrow-band model for radiation calculations in a combustion environment. NIST Technical Note 1402, 1993.

[19] R. S. Barlow, A. N. Karpetis, J. H. Frank, and J. Y. Chen. *Combustion and Flame*, 127 (2001) 2102–2118.

[20] G. L. Hubbard and C. L. Tien. *Journal of Heat Transfer*, 100 (1978) 235–239.

[21] J. B. Moss and I. Aksit. *Proceedings of the Combustion Institute*, 31 (2007) 3139–3146.

[22] H. Pitsch. Flamemaster: A C++ computer program for 0D combustion and 1D laminar flame calculations. 1998.

[23] C. D. Pierce and P. Moin. *Physics of Fluids*, 10 (1998) 3041.

[24] S. Ghosal, T. S. Lund, P. Moin, and K. Akselvoll. *Journal of Fluid Mechanics*, 286 (1995) 229–255.

[25] R. J. Santoro, H. G. Semerjian, and R. A. Dobbins. *Combustion and Flame*, 51 (1983) 203–218.

[26] K. C. Smyth. http://www.bfrl.nist.gov. 1999.

[27] Thomas K. Blanchat. Characterization of the air source and the plume source at FLAME. In *SAND 2001-2227*, 2001.

[28] SR Tieszen, TJ O'Hern, RW Schefer, EJ Weckman, and RW Schefer. *Combustion and Flame*, 139 (2004) 126–141.

[29] H. Koo, J. C. Hewson, S. P. Domino, and R. C. Knaus. Model sensitivities in LES predictions of buoyant methane fire plumes. In *Western States Section of the Combustion Institute Fall Meeting*, 2017.